# The 2004 $M_w$6.0 Parkfield, California, earthquake: Inversion of near-source ground motion using multiple data sets

Susana Custódio,[1,2] Pengcheng Liu,[2] and Ralph J. Archuleta[1,2]

[1] On 28 September 2004, the $M_w$6.0 Parkfield earthquake became the most densely recorded earthquake for near-source ground-motion. To infer the kinematic nature of this event we invert the strong-motion data. The non-linear global inversion yields slip amplitude, slip rake, average rupture velocity, and rise time over the fault. By using subsets of the data, we study the dependence of the kinematic solutions on data input. The inversions reveal that the slip amplitude was less than 0.65 m and outline two major areas of slip; one that laterally surrounds the hypocenter, preferentially extending to its SE; the other 10 to 20 km NW of the hypocenter, at a depth between 2 and 8 km. The slip amplitude we obtain for each point on the fault varies less than 0.15 m depending on data set used; the rake angle variability is less than 40°. **Citation:** Custódio, S., P. Liu, and R. J. Archuleta (2005), The 2004 $M_w$6.0 Parkfield, California, earthquake: Inversion of near-source ground motion using multiple data sets, *Geophys. Res. Lett.*, *32*, L23312, doi:10.1029/2005GL024417.

## 1. Introduction

[2] The San Andreas Fault is the primary fault that accommodates right-lateral tectonic motion taking place between the Pacific plate and the North American plate. The Parkfield section of the San Andreas Fault marks the transition between a seismically locked zone, to the SE, and a region of creep, to the NW. The locked segment produces large earthquakes spaced approximately 150 years apart [*Sieh*, 1978]. In contrast, frequent small earthquakes ($M_w$ < 5) and significant surface displacement [*Lisowski and Prescott*, 1981] characterize the creeping zone. Between these two seismically distinct zones is the Parkfield section. During historical time it has released six earthquakes, each about $M_w$6. *Bakun and McEvilly* [1984] proposed the concept of the Parkfield characteristic earthquake: an event that would repeat every 22 years, that would nucleate on the same hypocenter, and that would rupture the same area of the fault. Their model predicted that a Parkfield earthquake was due between 1983 and 1993, which led to the Parkfield Prediction Experiment [*Bakun and Lindh*, 1985]. The predicted Parkfield earthquake did occur 28 September 2004, becoming the most extensively recorded earthquake in the near-source region.

[3] In this paper we build a kinematic rupture model for the 2004 Parkfield event by inverting strong-motion seismic data. The abundance of high-quality data allowed for a study of how resulting rupture models depend on the data that is used. We used two techniques to determine how robust the model is: (1) Data from a given subset of stations were inverted and the resulting rupture model was used to predict ground motion at the remaining stations; and (2) data from 12 subsets of stations were inverted. The 12 resulting rupture models were then used to study the degree to which our solutions depend on the chosen data input.

## 2. Kinematic Inversion

[4] The nonlinear global inversion method of *Liu and Archuleta* [2004] was used to find a kinematic rupture model for the Parkfield earthquake. The rupture model is defined by four source parameters on a grid of points covering the assumed fault plane - slip amplitude, slip rake, rise time and average rupture velocity between hypocenter and each node. The inversion procedure of *Liu and Archuleta* [2004] relies on a simulated annealing algorithm to efficiently find a model that best fits the observed data. The purpose of the inversion is to minimize a misfit function [*Liu and Archuleta*, 2004, equation (9b)] that measures the difference between synthetic and observed velocity waveforms. In addition, the misfit function imposes smoothness and seismic moment constraints on the model being derived.

[5] Green's functions are computed at a 500 m × 500 m spacing using the FK method of *Zhu and Rivera* [2002]. The input to the Green's functions computation is a layered velocity structure that is different on each side of the fault. Thus we take into account the velocity contrast between the granitic Salinian block west of the fault (faster) and the Franciscan terrain east of the fault (slower). This bilateral 1D velocity model (Table 1) was adapted from the 3D velocity models of *Eberhart-Phillips and Michael* [1993] and *Thurber et al.* [2003]. Source parameters are inverted for on a 2 km × 2 km grid. Slip ($s(t)$) at each node is described by a function that initially accelerates rapidly, then progressively slows down (Equation 1). The rise time (T) is split into an accelerating (T1) and a decelerating (T2) rise times, such that T = T1 + T2. T1 and T2 are two independent parameters in the inversion. Source parameters and Green's functions undergo bilinear interpolation onto a 167 m × 167 m grid, which is imposed on the fault surface.

$$\frac{ds}{dt} = \begin{cases} A\left[\sin\left(\frac{t}{T_1}\frac{\pi}{2}\right)\right] & \text{if } 0 < t < T_1 \\ \frac{A}{2}\left[1 + \cos\left(\frac{t - T_1}{T_2}\pi\right)\right] & \text{if } T_1 < t < T_1 + T_2 \end{cases} \quad (1)$$

---

[1]Department of Earth Science, University of California, Santa Barbara, California, USA.

[2]Institute for Crustal Studies, University of California, Santa Barbara, California, USA.

where

$$\frac{1}{A} = \frac{2T_1}{\pi} + \frac{T_2}{2}$$

[6] Grid size and velocity structure resolution impose an upper boundary on the frequencies of ground-motion that can be modeled. Instrument sensitivity limits the lowest frequencies that are recorded. Consequently, the models presented here aim solely at explaining shaking at frequencies between 0.16 Hz and 1.0 Hz. We invert velocity waveforms that we obtain after integrating the acceleration records and band-pass filtering the resulting velocity data. Even though some records contain spectral information below 0.16 Hz, for simplicity we choose a frequency pass-band that is common to all records.

[7] Because no evidence of surface break was found immediately after the earthquake [*Langbein et al.*, 2005], we allow no slip shallower than 500 m. The hypocenter in our model is at 35.817°N, 120.365°W and 8.1 km depth. We model the fault as striking 141°SE and dipping 89°SW, the ruptured fault area is 40 km long and 15 km deep. This fault area coincides with aftershock locations. Given that most of the energy in a strike-slip earthquake is released on the horizontal plane, we downweight the contribution of vertical data to the misfit function by a factor of ten in relation to horizontal data.

## 3. Inversion of Data Subsets

[8] This study uses the largest volume of near-source data available that satisfies minimum requirements: frequency response of the instrument must be flat above 0.16 Hz; S-arrival must be clear (for waveform alignment); and recordings must be taken within 32 km of the epicenter. Strong-motion data from 43 three-component
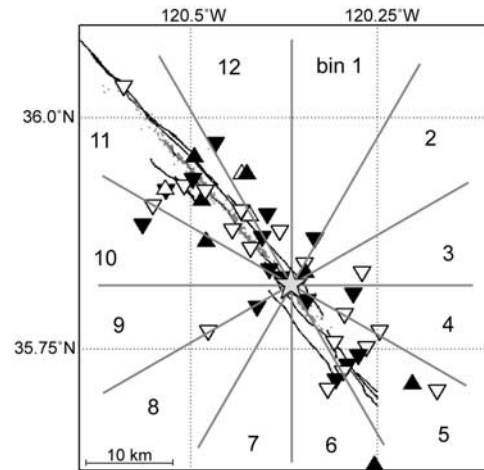


**Figure 1.** Group A - 22 stations (black). Group B - 21 stations (white). Station codes can be found in the auxiliary material. Inverted triangles - CGS stations; triangles - USGS stations; small gray dots - aftershocks [*Hardebeck and Michael*, 2004]; star - epicenter. Group B and Group A are equivalent in terms of number of stations, station azimuthal distribution, and distance between station and fault.

seismographs (9 USGS digital recorders and 34 CGS primarily analog recorders; see *Shakal et al.* [2005] for a complete discussion of these data) fulfill these conditions. We inverted 12 data subsets (available in the auxiliary material[1]) in order to investigate the influence of data input on resulting models. Subsets were constructed to be equivalent, in that each subset should contain a similar number of stations, and the distribution of stations in terms of azimuth to the epicenter and distance to the fault plane should be similar. Twelve subsets were outlined in the following way:

[9] 1. The total 43 stations were divided into Group A and Group B (Figure 1). The two groups are equivalent according to the definition established above.

[10] 2. Both groups were divided azimuthally around the epicenter to form 12 bins (see the auxiliary material). Note that two bins of a same number (e.g., bin 1 including stations at azimuths to the epicenter between 0° and 30°) can be interchanged between Group A and Group B without altering the overall station distribution of the groups.

[11] 3. Bins of the same number are alternately exchanged between Group A and Group B, thus creating new subsets. Each time a subset is created, a complementary subset, with the remaining stations, is also created. Therefore all data are used the same number of times.

[12] Next, we invert the 12 data subsets to obtain 12 rupture models (Figure 2). The final value of the misfit function is comparable for all models, ranging from 0.32 to 0.39. Seismic moment for the 12 slip models is approximately $1.08 \times 10^{18}$Nm. Because the model considers the area of rupture to be larger than expected for a $M_w$6.0 earthquake, seismic moment must be constrained;

**Table 1.** Velocity 1D Structure[a]

| Thickness, km | Density, g/cm³ | Vp, km/s | Vs, km/s | Qp | Qs |
|---|---|---|---|---|---|
| | | *SW* | | | |
| 1.0 | 2.0 | 2.0 | 1.1 | 70 | 35 |
| 1.0 | 2.3 | 3.5 | 2.0 | 140 | 80 |
| 1.0 | 2.3 | 4.5 | 2.5 | 300 | 200 |
| 0.5 | 2.5 | 5.2 | 3.0 | 390 | 230 |
| 2.3 | 2.7 | 5.7 | 3.2 | 500 | 260 |
| 8.3 | 2.7 | 6.2 | 3.6 | 500 | 300 |
| 3.0 | 2.8 | 6.8 | 3.6 | 510 | 300 |
| 3.3 | 2.8 | 6.8 | 4.3 | 510 | 550 |
| - | 2.8 | 7.3 | 4.3 | 800 | 550 |
| | | *NE* | | | |
| 1.0 | 2.0 | 2.0 | 1.1 | 70 | 35 |
| 0.8 | 2.3 | 3.5 | 2.2 | 140 | 80 |
| 0.3 | 2.3 | 4.2 | 2.8 | 300 | 200 |
| 1.3 | 2.3 | 4.8 | 2.7 | 320 | 200 |
| 0.5 | 2.3 | 5.2 | 2.8 | 380 | 200 |
| 4.4 | 2.7 | 5.3 | 3.2 | 380 | 250 |
| 4.4 | 2.8 | 5.7 | 3.7 | 500 | 290 |
| 4.8 | 2.8 | 6.5 | 3.8 | 500 | 290 |
| 2.8 | 2.8 | 6.7 | 4.3 | 510 | 530 |
| - | 2.8 | 7.3 | 4.3 | 800 | 550 |

[a]Each horizontal layer is characterized by its thickness, density, P- and S-wave velocity (Vp and Vs) and attenuation (1/Qp and 1/Qs).
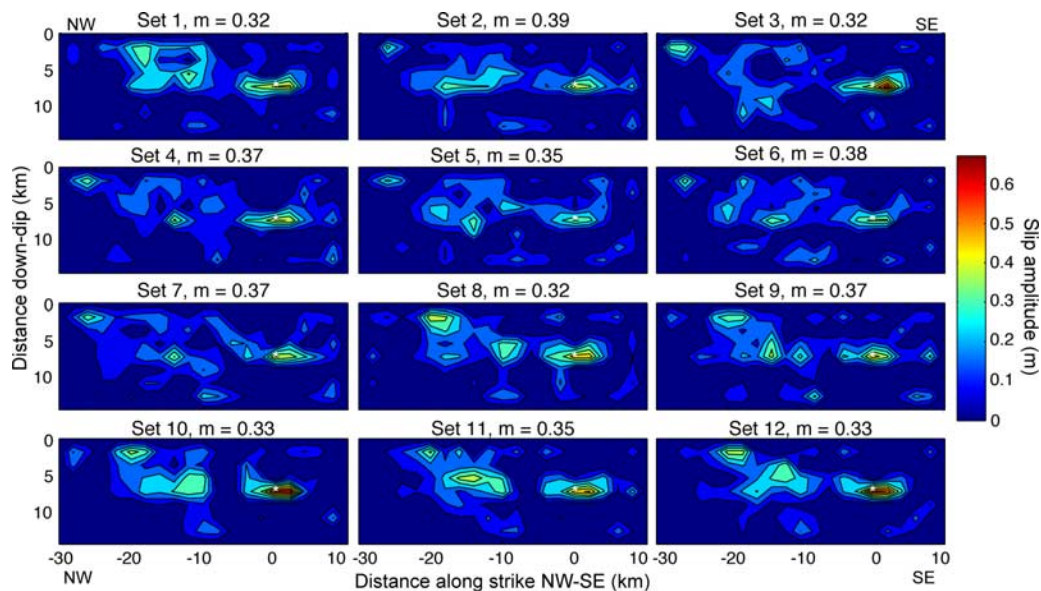
**Figure 2.** Models of final slip amplitude obtained by inversion of 12 different subsets of data. The misfit (*m*) is indicated above each slip distribution.

otherwise, patches of the fault with low slip amplitude contribute a spurious amount of seismic moment.

## 4. Rupture Model Discussion

[13] Each of the 12 models was found by inverting a given subset of stations. If we now take each model and generate ground-motion at the remaining stations, how well do the predicted waveforms fit the data? Figure 3 exemplifies that for predicted waveforms the misfit is approximately twice as much as the misfit for inverted waveforms. This increase in misfit for predicted ground motion suggests that wave propagation contributions, such as site effects or complexities of geological structure, and

artifacts of the inversion process itself, may have been mapped into the slip solutions.

[14] The average, standard deviation and coefficient of variance for the 12 models are shown on Figure 4. The source model that is obtained by averaging the 12 slip solutions (row B), although less detailed than each one of the 12 individual solutions, is close to the model that results from simultaneous inversion of the total available data (row A). Such similarity is to be expected given that each data record has the same weight in the derivation of both models. The coherent features between the 12 models are: slip amplitude less than 0.65 m; zone of greatest slip amplitude extending laterally around the hypocenter, preferentially to its SE; secondary zone of large slip
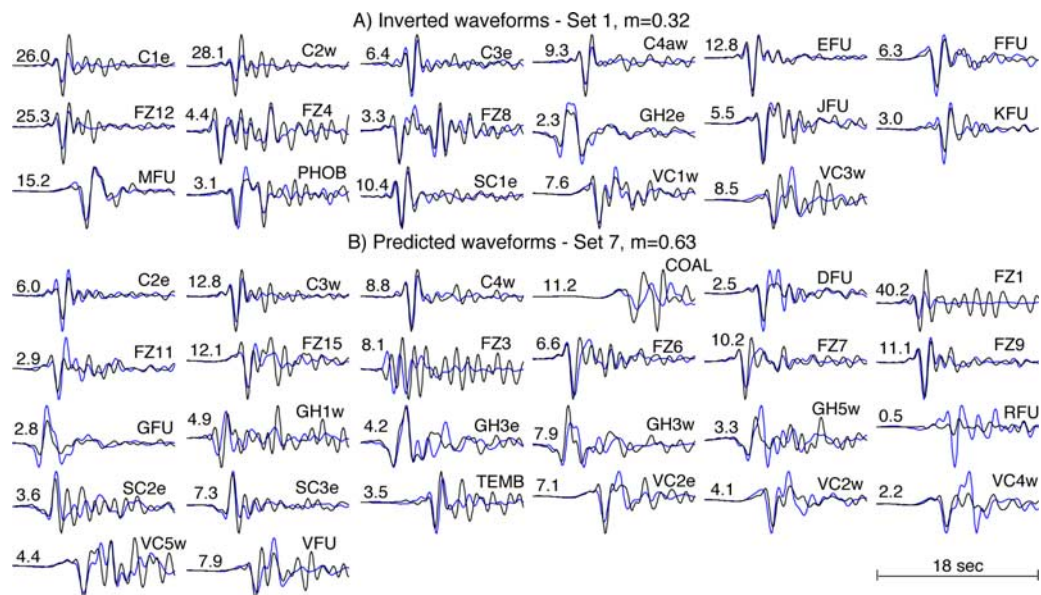


**Figure 3.** Comparison between transverse velocity component of synthetics (blue line) and (a) Set 1 - data used in the inversion; (b) Set 7 - data not used in the inversion (black line). Peak velocity (cm/s) of each record is shown on its upper-left corner, station code on its right-top corner.
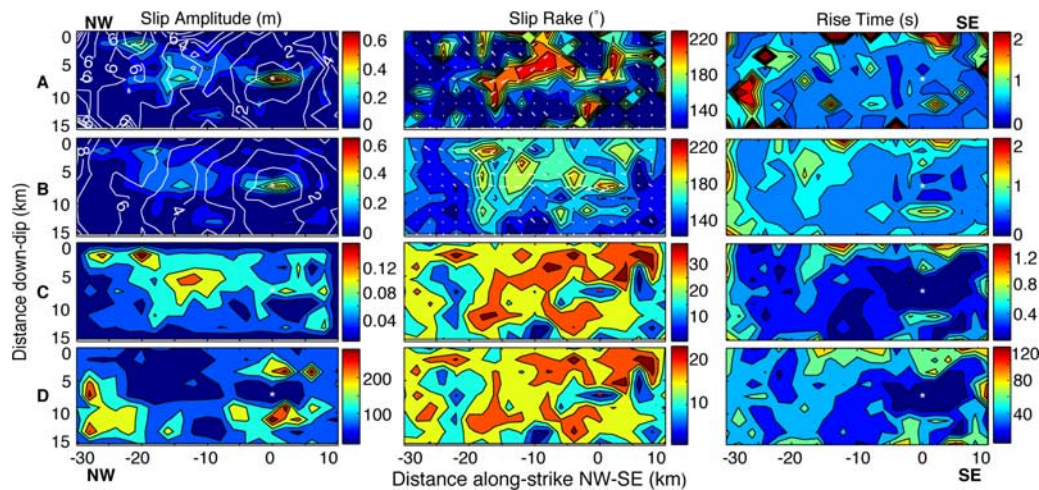
**Figure 4.** Source parameters. (left) Slip amplitude and rupture time (white lines are 1 sec contours); (middle) rake angle and slip vector field (white arrows); (right) rise time. (a) inversion of all available data; (b) average of 12 solutions; (c) standard deviation; and (d) coefficient of variance. The average retains only the coherent features from the 12 different models obtained with 12 data subsets. The standard deviation measures the difference between the average model and the 12 individual models. The coefficient of variance shows the percentage of variability of individual models with respect to the average. The asterisk marks the hypocenter.

amplitude 10 to 20 km NW of the hypocenter, at a depth between 2 and 8 km; small region of deep (13 km) slip 10 km NW of the hypocenter; rupture lasted approximately 10 sec; rise time lower than 1 sec over most of the fault.

[15] Figure 4c reveals that data input affects up to 0.15 m the slip amplitude solution. The coefficient of variance (Figure 4d) indicate that slip amplitude is poorly resolved in areas of low slip. Rake angle dependence on data set is generally less than 40°. Despite the small standard deviation of the rise time, it is not well resolved; our maximum frequency is only 1 Hz, so it will be difficult to image rise times below 1 sec. All source parameters are best resolved in the hypocentral region. In particular, we cannot sharply define the contours of slip amplitude to the NW of the hypocenter.

## 5. Conclusions

[16] We have derived a model for the time-space slip distribution during the 2004 Parkfield earthquake from strong-motion near-source data. We have also been able to quantify the standard deviation of the rupture model. Although this study used a vast quantity of data, we suggest that similar studies may be conducted with smaller data sets. In such cases, subsets can be obtained by subtracting one or two stations from the total number of stations. The prediction of ground motion at stations that are not used in the inversion indicates that various non-source effects are being mapped into individual slip solutions. Nevertheless, seismic phases of predicted waveforms are well constrained, which suggests that all models obtained are reasonably adequate. Despite some variability between models that are obtained using multiple data subsets, common features can be identified. Only these persistent features should be considered accurate when concluding about earthquake and fault dynamics.

## References

Bakun, W. H., and A. G. Lindh (1985), The Parkfield, California, earthquake prediction experiment, *Science*, *229*(4714), 619–624.

Bakun, W. H., and T. V. McEvilly (1984), Recurrence models and Parkfield, California, earthquakes, *J. Geophys. Res.*, *89*, 3051–3058.

Eberhart-Phillips, D., and A. J. Michael (1993), Three-dimensional velocity structure, seismicity, and fault structure in the Parkfield region, central California, *J. Geophys. Res.*, *98*, 15,737–15,758.

Hardebeck, J. L., and A. Michael (2004), Earthquake locations before and after the 2004 M6.0 Parkfield earthquake, *Eos Trans. AGU*, *85*(47), Fall Meet. Suppl., Abstract S51C-0170W.

Langbein, J., R. Borcherdt, D. Dreger, J. Fletcher, J. L. Hardebeck, M. Hellweg, C. Ji, M. Johnston, J. R. Murray, R. Nadeau, M. J. Rymer, and J. Treiman (2005), Preliminary report on the 28 September 2004, M6.0 Parkfield, California, earthquake, *Seismol. Res. Lett.*, *76*, 10–26.

Lisowski, M., and W. H. Prescott (1981), Short-range distance measurements along the San Andreas fault system in central California, 1975 to 1979, *Bull. Seismol. Soc. Am.*, *71*, 1607–1624.

Liu, P., and R. J. Archuleta (2004), A new nonlinear finite fault inversion with three-dimensional Green's functions: Application to the 1989 Loma Prieta, California, earthquake, *J. Geophys. Res.*, *109*, B02318, doi:10.1029/2003JB002625.

Shakal, A., V. Graizer, M. Huang, R. Borcherdt, H. Haddadi, K. Lin, C. Stephens, and P. Roffers (2005), Preliminary analysis of strong-motion recordings from the 28 September 2004 Parkfield, California earthquake, *Seismol. Res. Lett.*, *76*, 27–39.

Sieh, K. E. (1978), Slip along the San Andreas Fault associated with the great 1857 earthquake, *Bull. Seismol. Soc. Am.*, *68*, 1421–1448.

Thurber, C., S. Roecker, K. Roberts, M. Gold, L. Powell, and K. Rittger (2003), Earthquake locations and three-dimensional fault zone structure along the creeping section of the San Andreas fault near Parkfield, CA: Preparing for SAFOD, *Geophys. Res. Lett.*, *30*(3), 1112, doi:10.1029/2002GL016004.

Zhu, L., and L. A. Rivera (2002), A note on the dynamic and static displacements from a point source in multilayered media, *Geophys. J. Int.*, *148*, 619–627, doi:10.1046/j.1365-246X.2002.01610.x.

————————————
R. J. Archuleta and S. Custódio, Department of Earth Science, University of California, Santa Barbara, CA 93106-1100, USA. (susana@crustal.ucsb.edu)

P. Liu, Institute for Crustal Studies, University of California, Girvetz Hall 1140P, Santa Barbara, CA 93106, USA.